

AD _____

Award Number: W81XWH-04-1-0594

TITLE: Pre-Clinical and Clinical Evaluation of High Resolution, Mobile Gamma Camera and Positron Imaging Devices

PRINCIPAL INVESTIGATOR: David R. Gilland, Ph.D.

CONTRACTING ORGANIZATION: University of Florida
Gainesville, FL 32611

REPORT DATE: November 2007

TYPE OF REPORT: Annual

PREPARED FOR: U.S. Army Medical Research and Materiel Command
Fort Detrick, Maryland 21702-5012

DISTRIBUTION STATEMENT: Approved for Public Release;
Distribution Unlimited

The views, opinions and/or findings contained in this report are those of the author(s) and should not be construed as an official Department of the Army position, policy or decision unless so designated by other documentation.

REPORT DOCUMENTATION PAGE

Form Approved
OMB No. 0704-0188

Public reporting burden for this collection of information is estimated to average 1 hour per response, including the time for reviewing instructions, searching existing data sources, gathering and maintaining the data needed, and completing and reviewing this collection of information. Send comments regarding this burden estimate or any other aspect of this collection of information, including suggestions for reducing this burden to Department of Defense, Washington Headquarters Services, Directorate for Information Operations and Reports (0704-0188), 1215 Jefferson Davis Highway, Suite 1204, Arlington, VA 22202-4302. Respondents should be aware that notwithstanding any other provision of law, no person shall be subject to any penalty for failing to comply with a collection of information if it does not display a currently valid OMB control number. **PLEASE DO NOT RETURN YOUR FORM TO THE ABOVE ADDRESS.**

1. REPORT DATE (<i>DD-MM-YYYY</i>) 01-11-2007		2. REPORT TYPE Annual		3. DATES COVERED (<i>From - To</i>) 13 May 2006 - 13 Oct 2007	
4. TITLE AND SUBTITLE Pre-clinical and Clinical Evaluation of High Resolution, Mobile Gamma Camera and Positron Imaging Devices				5a. CONTRACT NUMBER	
				5b. GRANT NUMBER W81XWH-04-1-0594	
				5c. PROGRAM ELEMENT NUMBER	
6. AUTHOR(S) David R. Gilland, Ph.D. E-Mail: gilland@ufl.edu				5d. PROJECT NUMBER	
				5e. TASK NUMBER	
				5f. WORK UNIT NUMBER	
7. PERFORMING ORGANIZATION NAME(S) AND ADDRESS(ES) University of Florida Gainesville, FL 32611				8. PERFORMING ORGANIZATION REPORT NUMBER	
9. SPONSORING / MONITORING AGENCY NAME(S) AND ADDRESS(ES) U.S. Army Medical Research and Materiel Command Fort Detrick, Maryland 21702-5012				10. SPONSOR/MONITOR'S ACRONYM(S)	
				11. SPONSOR/MONITOR'S REPORT NUMBER(S)	
12. DISTRIBUTION / AVAILABILITY STATEMENT Approved for Public Release; Distribution Unlimited					
13. SUPPLEMENTARY NOTES					
14. ABSTRACT: The objective of this project is to design, build and evaluate a compact and mobile gamma and positron imaging camera. This imaging device has several advantages over conventional systems: (1) greater flexibility in positioning with respect to the target organ for improved spatial resolution and sensitivity, (2) the ability to image patients who cannot be transported to a radiology suite, (3) the potential for improved cost effectiveness for organ-specific imaging tasks compared with larger, general purpose imaging systems. Simulation studies have demonstrated the potential image quality that can be produced with this device operating in either dual gamma, coincidence mode or single gamma mode. Over the past year, the following tasks have been completed: mechanical testing of the system gantry, fabrication of the detectors, integration of the detectors and system gantry, and basic system performance evaluation using phantoms. The performance evaluation included the basic metrics of imaging performance including spatial resolution, system sensitivity, energy resolution and count rate capability. This report details the results of these measurements. The results, in summary, show the promise of this unique imaging device to provide essential diagnostic information for critically ill patients. Additional effort during the past year has focused on the preparation of the human subjects research protocol in anticipation of the further evaluation of this imaging system on clinical patients.					
15. SUBJECT TERMS PET, SPECT, Cardiac Imaging, Detectors					
16. SECURITY CLASSIFICATION OF:			17. LIMITATION OF ABSTRACT	18. NUMBER OF PAGES	19a. NAME OF RESPONSIBLE PERSON
a. REPORT	b. ABSTRACT	c. THIS PAGE			USAMRMC
U	U	U	UU	22	19b. TELEPHONE NUMBER (<i>include area code</i>)

Table of Contents

Introduction	4
Body	4
Key Research Accomplishments	7
Reportable Outcomes	7
Conclusions	7
Appendices	8

INTRODUCTION

The objective of this project is to design, build and evaluate a compact and mobile camera for gamma and positron imaging. This imaging device has several advantages over conventional systems: (1) improved spatial resolution and sensitivity due to greater flexibility in positioning with respect to the target organ, (2) the ability to image patients who cannot be transported to a radiology suite, (3) the potential for improved cost effectiveness for organ-specific imaging tasks compared with larger, general purpose imaging systems. The basic performance of this unique imaging device was evaluated using physical phantoms, and the results of this evaluation are provided in this report. Additional effort during the past year has focused on the preparation of the human subjects research protocol in anticipation of the further evaluation of this imaging system on clinical patients.

One of the two detectors in the original system design was extensively damaged during shipping. The circumstances during shipping indicate that there was gross negligence by United Parcel Service (UPS) in its material handling, and UF is currently pursuing legal efforts to hold UPS monetarily accountable. These events have not impeded us from achieving the aims of this project. As a result, we have focused our imaging approach to operate in single photon detection mode, which requires the use of only one detector.

BODY

System Assembly and Mechanical Performance Evaluation (tasks 12-13 of Project Timeline in Appendix 1)

The electro-mechanical gantry allows the detectors to be transported within a hospital and has been designed for precise positioning of the detectors with respect to the patient. The gantry system has been designed to position the detectors for PET or SPECT acquisition under the challenging conditions of the bedside environment. Low profile legs slide beneath ICU beds for stable support. The detectors mount to the rails of a linear bearing set that allows precise horizontal detector motion. Vertical detector motion is motor-driven using electronic motion control modules. Detector pivoting provides the additional, necessary motion dimension. The linear motions and pivot angle are digitally encoded for input to the reconstruction software. In PET mode, the detectors assume a 180 deg. opposing orientation; in SPECT mode, the two detectors can assume a variable angle orientation (90-180 deg.) and orbit the anterior of the patient.

The detectors were delivered to UF from Jefferson Lab in April 2007, and an evaluation of the mechanical capabilities of the system with detectors mounted has been performed. The added weight of the detectors has not impeded the mechanical performance of the system. As shown in Fig. 1, the gantry can position the detectors in an anterior/posterior, lateral or both anterior orientations. This work, including an initial imaging performance evaluation, was accepted for presentation at the 2007 IEEE Medical Imaging Conference and is included in this report in Appendix 2.



Fig. 1: Photograph of system gantry with actual detectors mounted. Detectors are positioned in anterior/posterior (left), lateral (middle), and both anterior (right) orientations

Imaging Performance Evaluation with Phantoms (tasks 14-15)

The basic imaging performance of the integrated system has been performed. This work has been accepted for presentation at the 2007 IEEE Nuclear Science Symposium and Medical Imaging Conference. A copy of the conference paper has been included in this report as Appendix 2. A summary of this paper is presented here.

The basic imaging performance metrics that were measured include energy resolution, spatial resolution, system sensitivity, and count rate capability. These measurements were performed using both Tc-99m (140 keV photon energy) and F-18 (511 keV). This system has been designed to satisfactorily image tracers at both of these photon energies.

Energy Resolution. The results of the energy resolution measurements are shown in Fig. 2. The measured % full-width-at-half-maximum (FWHM) was found to be %42 for 140 keV and 23% for 511 keV.

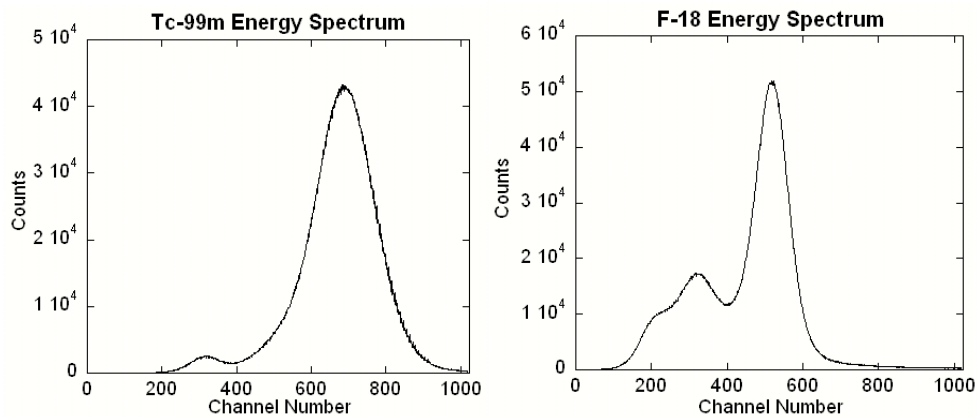


Fig. 2. Measured energy spectra for Tc-99m and F-18.

Spatial Resolution. Using a 1 mm slit phantom, the measured intrinsic (without collimator) spatial resolution was 0.59 cm FWHM. The system (with collimator) spatial resolution was measured for 140 keV and 511 keV using low energy and high energy collimators, respectively. A line source, consisting of a capillary tube filled with Tc-99m or F-18 solution, was imaged at 10, 20 and 30 cm from the collimator face. From these images, profiles were obtained perpendicular to the line to generate the line spread functions (LSF's). These are shown in Fig. 3.

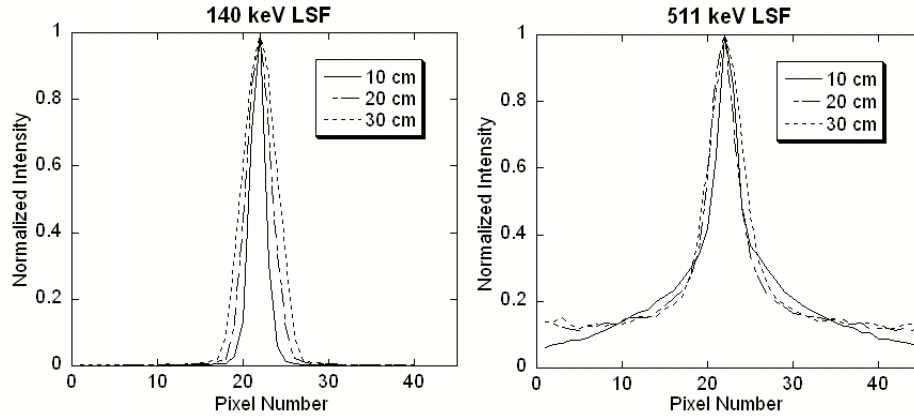


Fig. 3. Measured spatial resolution (LSF's) for 140 keV and 511 keV

The LSF's from 511 keV data demonstrate “tails” in the distribution due to collimator septa penetration of the high energy photons. In order to reduce the impact of these tails on the FWHM measurement, a constant that approximated the height of the tails was subtracted from the distributions before the FWHM measurement. These system spatial resolution results are summarized in Table I. As the table indicates, a reasonable agreement has been found between the theoretical and measured spatial resolution for 14 keV and 511 keV (with subtraction).

TABLE I. SYSTEM SPATIAL RESOLUTION MEASUREMENTS (FWHM in cm)

	b [cm]	No Subtraction	With Subtraction	Theoretical	% Deviation
140 keV	10	1.14	-	0.99	14.7
	20	1.64	-	1.57	4.5
	30	2.35	-	2.18	7.8
511 keV	10	1.54	1.14	1.03	50.0 / 11.1
	20	1.93	1.62	1.56	23.7 / 3.8
	30	2.64	2.03	2.13	23.9 / -4.7

System Sensitivity. Using calibrated point source acquisitions, the system sensitivity for Tc-99m was found to be 3.1 counts per second per μCi and for F-18 was found to be 0.48 counts per second per μCi . The sensitivity measurement for F-18 used a region-of-interest that excluded the uncollimated detected counts.

Count Rate Capability. The maximum measured count rate of the detector was 1.56×10^5 counts per second for 511 keV (at 275 μCi of activity) and 1.46×10^5 counts per second for 140 keV (at 135 μCi of activity).

Establish Human Subjects Research Protocol (tasks 16-17)

We have prepared a draft of a Human Subjects Research Protocol in anticipation of the further evaluation of this imaging system on clinical patients. This protocol will first be reviewed by the Regulatory Compliance Specialist at TATRC and will then be submitting to the local Institutional Review Board at the University of Florida. A copy of this draft protocol is included in Appendix 4 of this report.

KEY RESEARCH ACCOMPLISHMENTS

I. System Assembly and Mechanical Performance Evaluation Completed (*tasks 12-13*)

- Detectors integrated with system gantry
 - mechanical integration including linear translation and rotations
 - electrical integration including translation position encodings and rotation angle encodings
- Mechanical Performance Evaluation: demonstration of satisfactory detector positioning:
 - orbiting the anterior of the patient
 - detector positioning beneath patient bed

II. Basic Imaging Performance Evaluation Completed (*tasks 14-15*)

- Energy resolution
- Spatial resolution
 - Intrinsic
 - System
- System Sensitivity
- Count rate capability

III. Preparation of Human Subjects Research Protocol (*task16-17*)

REPORTABLE OUTCOMES (since last annual report)

Presentations:

1. Majewski S, Gunning W, Hammond R, Kross B, Smith M, Popov V, Proffitt J, Weisenberger A, Wojcik R, and Gilland D. Development and Evaluation of Detector Heads and Readout for a Mobile Cardiac Imager System. Presented at: 2006 IEEE Nuclear Science Symposium and Medical Imaging Conference, October 29 – Nov. 4, 2006, San Diego, California.

Submitted Conference Proceedings:

1. Studenski, M.T., Parker, J.G., Gilland, D.R., Majewski, S., Hammond, W., Performance Evaluation of a Small Field-of-View, Mobile PET/SPECT System. Accepted: Proceedings of the 2007 IEEE Nuclear Science Symposium and Medical Imaging Conference. (**Included as Appendix 2 in this report**)
2. Weisenberger, A.G., Majewski, S., Gilland, D.R., Hammond, W., Kross, B., Popov, V., Proffitt, J., McKisson, J, Smith, M.F., Implementation of a Mobile Cardiac PET Imager for the Emergency Room and Intensive Care Unit. Accepted: Proceedings of the 2007 IEEE Nuclear Science Symposium and Medical Imaging Conference. (**Included as Appendix 3 in this report**)

CONCLUSIONS

During the past year, we have made progress as follows: delivery of the detectors Jefferson Lab to University of Florida, mechanical and electrical integration of the detectors with the system gantry, mechanical performance evaluation of the integrated system, and basic imaging performance of the system. The integrated system demonstrated the ability to position the detectors for effective tomographic imaging in positron emission tomography (PET) or single

photon emission computed tomography (SPECT). The results of the basic imaging performance showed a reasonable match between the predicted and measured performance. Future work will involve an extended performance evaluation using anthropomorphic phantoms and tomographic image acquisitions.

The medical benefits that this device will bring promise to be substantial, not only for the military health care system but also for health care of the general population. This device will be capable of delivering critical diagnostic imaging (PET and SPECT) to patients who otherwise cannot benefit from these technologies. Also, this device potentially can be a cost effective alternative to conventional PET systems for cardiac imaging. Finally, with the accelerated growth in the development of imaging agents for PET and SPECT, there will be a greater need for novel and dedicated imaging devices, such as the device developed in this project.

APPENDICES

The following appendices are included as attachments to this report:

1. Project Timeline
2. Reprint of: Studenski, M.T., Parker, J.G., Gilland, D.R., Majewski, S., Hammond, W., Performance Evaluation of a Small Field-of-View, Mobile PET/SPECT System. Accepted: Proceedings of the 2007 IEEE Nuclear Science Symposium and Medical Imaging Conference.
3. Reprint of: Weisenberger, A.G., Majewski, S., Gilland, D.R., Hammond, W., Kross, B., Popov, V., Proffitt, J., McKisson, J, Smith, M.F., Implementation of a Mobile Cardiac PET Imager for the Emergency Room and Intensive Care Unit. Accepted: Proceedings of the 2007 IEEE Nuclear Science Symposium and Medical Imaging Conference.
4. Draft of Human Subjects Research Protocol

Appendix 1: Project Timeline

YEAR 1		
#	Activity	Duration (mos.)
Simulation Studies		
01	Simulation study I: determine required detector orbit	2
02	Simulation study II: determine spatial resolution, detection efficiency, count rate capability, reconstructed image quality	2
Gantry Design, Construction, and Evaluation		
03	Computer-aided design including intensive care bed	1
04	Specification of mechanical components	1
05	Fabrication of gantry using mock detectors	5
06	Evaluation of mechanical capabilities using mock detectors	5
Detectors Design, Construction, and Evaluation		
07	Optimization of data acquisition system for high count rate	3
08	Assembly of detector components	6
09	Planar detector performance evaluation	3
Image Reconstruction Algorithm Development		
10	Unconventional camera orbits/geometries	6
11	New iterative algorithms for limited angle data	6
YEAR 2		
System Assembly		
12	Mechanical, electrical assembly of detectors and gantry	2
13	Mechanical performance evaluation	2
Imaging Performance Evaluation with Phantoms		
14	Planar spatial resolution, detection sensitivity, count rate capability	3
15	Reconstructed image quality	4
Establish Human Subject Research Protocol		
16	Submit research protocol to local IRB's (UF and USF)	3
17	Identify patient population, coordinate with ICU staff	3

		Month															
		1	2	3	4	5	6	7	8	9	10	11	12				
YEAR 1		01		02													
		03	04	05				06									
		07			08						09						
		10								11							
	YEAR 2		12		13		14				15						
								16			17						

Performance Evaluation of a Small Field-of-View, Mobile PET/SPECT System

Matthew. T. Studenski, *Member, IEEE*, J.G. Parker, D.R. Gilland, S. Majewski, B. Hammond

Abstract— This paper reports on the initial performance evaluation of a small field-of-view, mobile PET/SPECT system for bedside imaging. The system was designed to move within a hospital to image patients who cannot easily be transported to a conventional PET or SPECT facility, for example, patients within an intensive care unit (ICU). The focus of the system is cardiac imaging in which both viability (^{18}F fluorodeoxyglucose; FDG) and perfusion ($^{99\text{m}}\text{Tc}$ Sestamibi) images are desired. This paper evaluates the capabilities of the mobile system for acquisitions at both 140 keV (Tc-99m) and at 511 keV (F-18) operated in single photon counting mode. Parameters evaluated were the planar and reconstructed SPECT spatial resolution, the intrinsic energy resolution, the sensitivity, and the count rate capability. Results demonstrate an intrinsic energy resolution of 42% at 140 keV and 23% at 511 keV, a planar intrinsic spatial resolution of 0.59 cm full width half-maximum (FWHM), an system spatial resolution at 10 cm of 1.01 cm FWHM at 140 keV and 1.33 cm FWHM at 511 keV, a reconstructed SPECT spatial resolution of 1.37 cm at 140 keV, a sensitivity of 3.1 counts $\mu\text{Ci}^{-1}\cdot\text{s}^{-1}$ at 140 keV and 0.48 counts $\mu\text{Ci}^{-1}\cdot\text{s}^{-1}$ at 511 keV, and a maximum count rate of 1.46×10^5 counts $\cdot\text{s}^{-1}$ at 140 keV and 1.56×10^5 counts $\cdot\text{s}^{-1}$ at 511 keV.

I. INTRODUCTION

The ability to bring an anatomical imaging system (mobile radiographic system or mobile C-arm fluoroscope) to a patient rather than the patient to the imaging system is commonplace in clinical radiology today. The University of Florida has developed an imaging system that allows functional imaging (SPECT and PET) to be brought to the patients who cannot be transported to a traditional facility. This mobile gantry system has been designed to position the detectors for PET or SPECT acquisition under the challenging conditions of the bedside environment. The company Segami Inc. does market a portable cardiac SPECT scanner, but it requires that the patient is seated [1].

The system consists of two compact detectors, each with approximately $25\times 25\text{ cm}^2$ detector areas, mounted on a mobile gantry system with a detachable computer and electronics rack (Fig. 1). The detectors (fabricated at Thomas Jefferson National Accelerator Facility [2]) consist of pixilated NaI(Tl)

(5 mm \times 5 mm \times 12.5 mm with 5.5 mm pitch). The photomultiplier tube readout uses position-sensitive PMTs with high-rate four analog outputs and arranged in a 4×4 array for each detector to form the $25\times 25\text{ cm}^2$ active detector area.

The gantry system includes low profile legs that slide beneath ICU beds for stable support. The detectors mount to the rails of a linear bearing set that allows precise horizontal detector motion. Vertical detector motion is motor-driven using electronic motion control modules. Detector pivoting provides the additional, necessary motion dimension for tomographic imaging. The linear motions and pivot angle are digitally encoded for input to the reconstruction software. In PET mode, the detectors assume an 180° opposing orientation and in SPECT mode, a single detector can assume any angular orientation and orbit the anterior of the patient (Fig. 1).

This paper reports on the performance evaluation of this imaging system operated in single photon detection mode for both 140 keV (Tc-99m) or 511 keV (F-18). The 511 keV SPECT approach, using a high energy collimator, has advantages over coincidence imaging because use with only one head allows for many more anterior projection angles to be obtained than with the detectors in the coincidence orientation since there is no need to orient a camera underneath the bed. Also, since the SPECT acquisition is performed anteriorly, this eliminates attenuation effects in the patient and the bed. Before any clinical images can be obtained the performance capabilities of these two modes of operation have to be quantified.

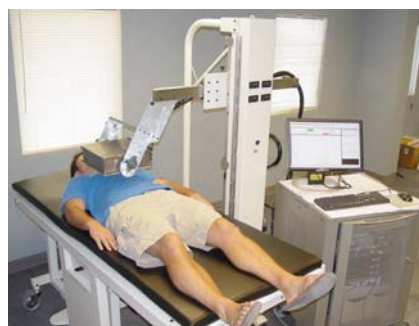


Fig. 1. Mobile gantry system in a bedside environment with the detector head in an anterior position for acquisitions in the single photon detection (SPECT) mode.

II. METHODS

The four metrics evaluated for the mobile system were intrinsic energy resolution, planar and reconstructed SPECT spatial resolution, sensitivity, and count rate capability for both 140 keV and 511 keV imaging. Switching the system

This work was supported by the United States Army Medical Research and Materiel Command under Award No. W81XWH-04-1-0594.

Matthew T. Studenski is with the Nuclear and Radiological Engineering Department at the University of Florida, Gainesville, FL 32611 USA. (telephone: 352-846-3066, e-mail: mstudens@ufl.edu).

J. G. Parker is with the Nuclear and Radiological Engineering Department at the University of Florida, Gainesville, FL 32611 USA. (telephone: 352-846-3066, e-mail: parkej@ufl.edu).

D. R. Gilland is with the Nuclear and Radiological and Biomedical Engineering Departments at the University of Florida, Gainesville, FL 32611 USA. (e-mail: gilland@ufl.edu).

between energies is done simply by adjusting the high voltage supplied to the photomultiplier tubes and by switching the collimator to low or high energy. The increased voltage is to maintain a linear relationship in the pulse height recorded by each photomultiplier tube. The different parameters between the high and low energy collimators are shown in Table I.

TABLE I. LOW ENERGY (140 keV) AND HIGH ENERGY (511 keV) COLLIMATOR PARAMETERS

	Low Energy	High Energy
Hole Shape	hexagonal	hexagonal
Thickness (l) [cm]	2.3	4.9
Hole Diameter (d) [mm]	1.5	2.3
Septal Thickness (t) [mm]	0.2	2.02

A. Energy Resolution

The energy resolution of the system was measured intrinsically (without collimator) with a point source positioned 75 cm from the detector face and 1.0×10^7 total counts acquired for each source. Using this geometry, energy spectra of the point sources were obtained. A 120 μCi source of Tc-99m (140 keV gamma) was imaged at the low energy setting and a 240 μCi source of F-18 (511 keV gamma) was imaged at the high energy setting. These activities were low enough to ensure that the detector did not exceed the maximum count rate. The peak channel and the FWHM of each spectrum were measured.

To determine a $\text{keV} \cdot \text{channel}^{-1}$ calibration factor for each energy setting, a 5 μCi source of Co-57 (122 keV gamma) was imaged at the low energy setting and a 65 μCi source of Cs-137 (662 keV gamma) was imaged at the high energy setting. The peak channel for each of these sources was measured and a $\text{keV} \cdot \text{channel}^{-1}$ factor was obtained for each energy setting. This calibration factor was used to convert the measured energy resolution (FWHM) into keV units.

B. Spatial Resolution

The intrinsic planar spatial resolution of the system was measured using a 1 mm wide slit phantom. A 490 μCi Tc-99m point source was positioned 75 cm from the detector face and 1×10^7 counts were obtained. Since almost all of the detector face was shielded, the count rate was not an issue.

The system planar spatial resolution at 140 keV and 511 keV was evaluated using line sources made of 1 mm diameter capillary tubes at distances of 10 cm, 20 cm, and 30 cm from the collimator face and oriented in both the X and Y directions. Profiles were taken across the images to obtain line spread functions (LSF) at each distance. 500 μCi of Tc-99m and 200 μCi of F-18 were used to obtain 5.0×10^5 counts at each distance and the FWHM was measured. For the 511 keV case, the FWHM was measured both with and without subtracting a constant from the LSF to compensate for the tails in the distribution due to septal penetration. The constant was computed from the average intensity of twenty pixels not contained in the peak. The measured FWHM was reported by averaging the X and Y directions. These results were then compared to the theoretical FWHM calculated using the

effective length of the collimator holes, the diameter of the holes, and the distance from of the collimator face [3].

Uniformity correction was applied to all the images acquired for spatial resolution measurements. The image used to uniformity correct each acquisition was the flood image acquired for the energy resolution evaluation at each respective energy. A 40% energy window was used for the 140 keV image and a 25% energy window was used for the 511 keV image.

A SPECT acquisition was performed on a Tc-99m point source to measure the reconstructed spatial resolution of the system at 140 keV. 2.5 mCi of Tc-99m in a syringe (essentially a point source) was imaged with 19 projections (every 10° from 0° – 180°) and 5×10^5 counts per projection. The Tc-99m in the syringe was centered in the field of view with a radius of rotation of 22 cm and a source-to-collimator distance of 15 cm. A filtered back-projection reconstruction algorithm with no smoothing filter was used to reconstruct the projections into a $45 \times 45 \times 45$ voxel image. A profile was taken across a transaxial slice of the reconstructed image and from this, the FWHM was measured.

C. Sensitivity

The extrinsic system sensitivity in terms of $\text{counts} \cdot \mu\text{Ci}^{-1} \cdot \text{s}^{-1}$ was evaluated using point sources of 240 μCi Tc-99m and 534 μCi F-18 suspended 30 cm from the collimator face. A 600 s acquisition with a 40% energy window for Tc-99m and a 25% energy window for F-18 was obtained of each source. For the 140 keV acquisition, the total number of counts in each pixel was summed to yield the total number of counts in the 600 s acquisition time. For the 511 keV acquisition, only a region of interest containing the source itself was summed to avoid counting events from septal penetration at the edge of the image. Using this data, the sensitivity of the detector at each energy setting was calculated.

D. Count Rate

The maximum intrinsic count rate was evaluated using 1.1 mCi F-18 and 535 μCi Tc-99m. Each source was suspended 30 cm from the detector face and 20 s acquisitions were obtained while the source decayed through several half lives. The number of counts per second (cps) minus the background was recorded at each time so the maximum count rate could be measured.

III. RESULTS

A. Energy Resolution

The energy spectrum from the Tc-99m and F-18 images can be seen in Fig. 2. The measured FWHM was 108 channels for the F-18 spectrum and 189 channels for the Tc-99m spectrum. The energy resolution for each energy setting was calculated by multiplying the calibration factor ($\text{keV} \cdot \text{channel}^{-1}$) to the FWHM obtained from each respective energy spectrum. The resulting energy resolutions were 42% at 140 keV and 23% at 511 keV.

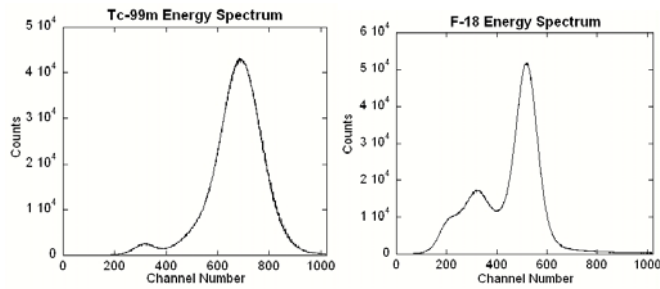


Fig. 2. Energy spectra obtained from 1×10^7 count acquisitions with Tc-99m and with F-18.

Results show that 140 keV SPECT imaging is possible but the degradation in energy resolution is a concern that will have to be addressed by implementing a new voltage distribution to the photomultiplier tube array that brings the energy resolution closer to 25% at 140 keV.

B. Spatial Resolution

The intrinsic spatial resolution of the detector was measured to be 0.59 cm FWHM. The reported crystal pixel pitch was 0.55 cm. One point of consideration was that the slit position could have been directly over a single pixel or partially over two pixels. Further experiments will clarify this issue and provide a more exact measurement. Fig. 3 shows the normalized intrinsic LSF from the slit phantom.

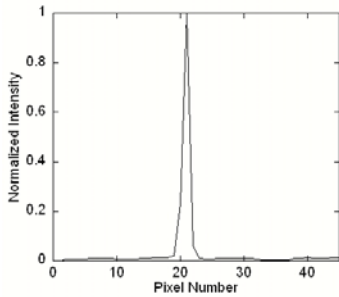


Fig. 3. Normalized intrinsic LSF measured using a 1 mm slit phantom.

Fig. 4 shows the normalized LSF for 140 keV and 511 keV in the X direction. Notice the tails from septal penetration in the 511 keV LSF.

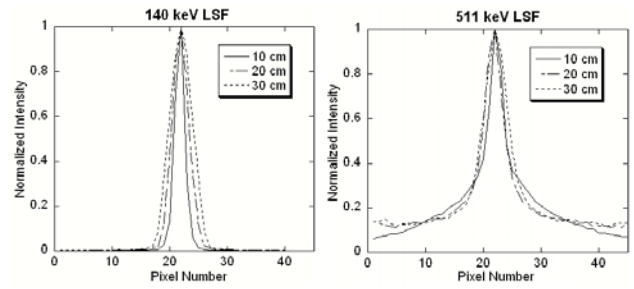


Fig. 4. Normalized LSFs obtained from 1 mm diameter capillary tube acquisitions of 5×10^5 counts at 10, 20, and 30 cm from the detector face at both 140 keV and 511 keV.

Fig. 5 shows the normalized LSF with the tails subtracted using the average pixel intensity from the tails (0.18). The measured FWHM of the LSF compared with theoretical values can be seen in Table II.

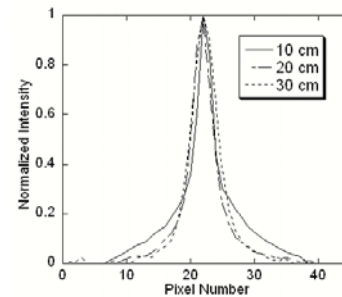


Fig. 5. Normalized LSFs of 1 mm capillary tube acquisitions at 511 keV with a constant (0.18) subtracted to eliminate septal penetration tails.

Table II shows that the tails from septal penetration caused significant degradation in the measured FWHM. Subtraction of the tails resulted in less deviation from the theoretical mean. To prove that the image degradation was actually a result of septal penetration and not scatter from surrounding materials, a simulation was run using the GATE software package [4], a front-end for the GEANT4 Monte Carlo simulation code [5], with the same geometry as the point source sensitivity acquisition but with no scattering materials surrounding the crystal (PMTs, gantry, detector box, etc.). Fig. 6 shows the real image (A) and the simulated image (B). The tails in the profile from the simulated image

TABLE II. SYSTEM SPATIAL RESOLUTION MEASUREMENTS (FWHM in cm)

	b [cm]	No Subtraction	With Subtraction	Theoretical	% Deviation
140 keV	10	1.14	-	0.99	14.7
	20	1.64	-	1.57	4.5
	30	2.35	-	2.18	7.8
511 keV	10	1.54	1.14	1.03	50.0 / 11.1
	20	1.93	1.62	1.56	23.7 / 3.8
	30	2.64	2.03	2.13	23.9 / -4.7

show that the spread in the LSF resulted from septal penetration and not from scatter. An interesting observation is the difference in PSF and LSF at 511 keV. The height of the penetration tail is higher in the LSF due to the contribution of

all parts of the line source to the tails. The point source does not have this extra source contribution and the tails only appear as a star pattern.

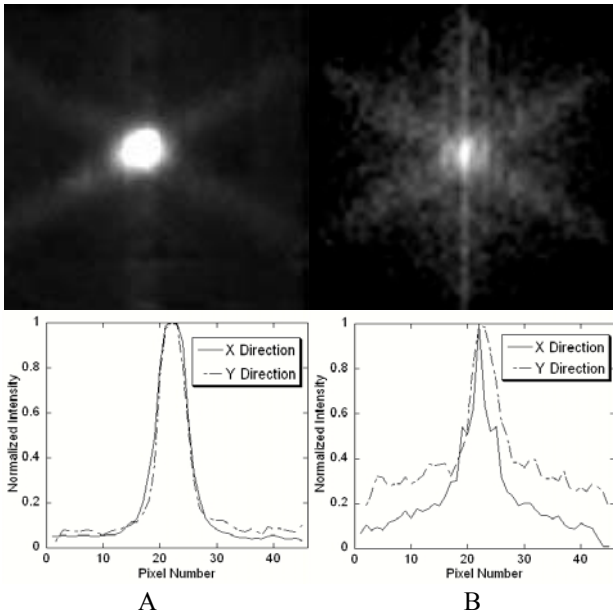


Fig. 6. Real (A) and simulated (B) 511 keV point source images with the corresponding PSFs in the X and Y directions.

Fig. 7 shows transaxial slice 45 from the reconstructed SPECT image of the Tc-99m syringe along with its corresponding PSF. The FWHM calculated from the PSF showed a FWHM of 1.37 cm.

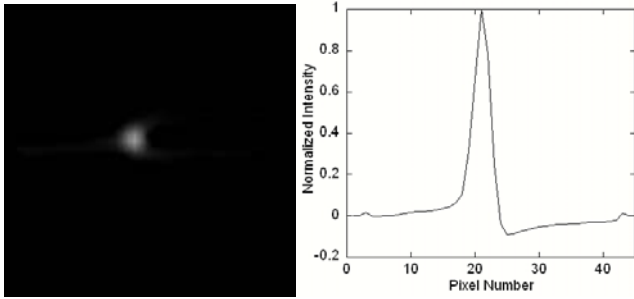


Fig. 7. Reconstructed transaxial slice 45 from a 19 angle SPECT acquisition of a Tc-99m point source and the corresponding PSF.

C. Sensitivity

From the total counts obtained in each image, the extrinsic sensitivity was calculated to be $3.1 \text{ counts} \cdot \mu\text{Ci}^{-1} \cdot \text{s}^{-1}$ for Tc-99m and $0.48 \text{ counts} \cdot \mu\text{Ci}^{-1} \cdot \text{s}^{-1}$ for F-18. The difference in sensitivity can be accounted for in two ways: the geometric sensitivity of the two collimators and the efficiency of the NaI crystal at each energy. The geometric sensitivity of the low energy collimator is two times higher than the high energy collimator and the linear attenuation coefficient of NaI at 140 keV is about 7.5 times higher than at 511 keV. These factors account for the much higher sensitivity of the system at 140 keV versus 511 keV.

D. Count Rate

The maximum intrinsic count rate of the detector was measured to be 1.56×10^5 cps at 511 keV and 1.46×10^5 cps at 140 keV. At this time of the maximum count rate, there was 275 μCi F-18 and 135 μCi Tc-99m present. The counting curves for 511 keV and 140 keV can be seen in Fig. 8.

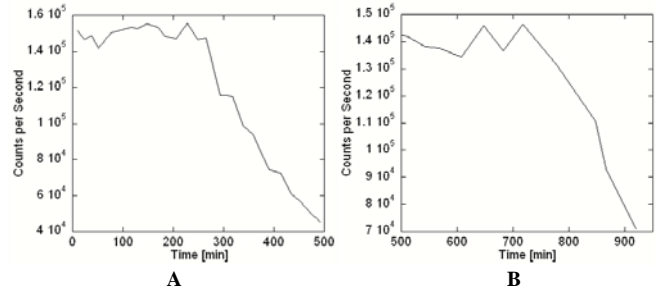


Fig. 8. Counting curves for 511 keV (A) and 140 keV (B) over several half-lives.

The saturation of the detector occurred at a lower activity for Tc-99m because of the higher sensitivity of the detector at this energy. More events were accumulated at a lower activity than at 511 keV. As expected, the detector saturated at an activity higher than the activity at the time of maximum count rate. Also, the images and energy spectra were distorted in the high activity acquisitions due to the saturation of the detector. In these distorted images, the peaks of the energy spectra were spread out and shifted from the normal channel. This meant that at very high activities the performance of the detector was reduced. For the most accurate images, the count rate must be kept below the maximum value.

IV. CONCLUSIONS AND FUTURE WORK

This unique system is capable of performing bedside SPECT imaging at both 140 keV and at 511 keV. Modifications in the system need to be made to improve energy resolution at 140 keV but proof of concept has been attained. Future work will involve multi-angle SPECT acquisitions at 511 keV to determine the reconstructed spatial resolution. Also, evaluation of the spatial resolution, sensitivity, count rate, and reconstructed spatial resolution of the PET capabilities of the system will also be part of ongoing research on this system.

REFERENCES

- [1] Segami Corporation, Columbia, MD.
- [2] S. Majewski, W. Gunning, R. Hammond, B. Kross, M. Smith, V. Popov, J. Proffitt, A. Weisenberger, R. Wojcik, and D. Gilland. Development and Evaluation of Detector Heads and Readout for a Mobile Cardiac Imager System. *2006 IEEE Nuclear Science Symposium and Medical Imaging Conference*.
- [3] S. Cherry, J. Sorenson, M. Phelps, *Physics in Nuclear Medicine*, 3rd ed. Philadelphia: Saunders, 2003.
- [4] S. Jan et al, "GATE: A Simulation Toolkit for PET and SPECT", *Physics in Medicine and Biology*, 2004; 49: 4543-4561.
- [5] Geant4 Collaboration (S. Agostinelli et al), "GEANT4: A Simulation Toolkit". *Nuclear Instruments and Methods in Physics Research*, 2003;506: 250-303.

Implementation of a Mobile Cardiac PET Imager for the Emergency Room and Intensive Care Unit

A.G. Weisenberger, S. Majewski, D. Gilland, W. Hammond, B. Kross, V. Popov, J. Proffitt, J. McKisson, and M. F. Smith

Abstract— Often emergency room and intensive care unit patients are in a condition too critical to be safely moved to a hospital's nuclear medicine suite to assess their cardiac function. To address this need we have built an economically practical mobile cardiac PET based imager for use in an intensive care/emergency room environment. The system is based on a pair of low profile 25 cm x 25 cm detector heads. Each head is structured in a modular fashion in that it utilizes an array of position sensitive photomultiplier tubes (PSPMTs) coupled to a NaI(Tl) crystal array. Sixteen Burle 85002-800 micro-channel plate-based PSPMTs are arranged to form each detector head resulting in a 25 cm x 25 cm field of view. The NaI(Tl) scintillating crystal array for each detector head is composed of 5 mm x 5 mm x 12.5 mm crystal elements spaced at a 5.5 mm step. The modular readout architecture has achieved over 100 kHz coincidence trigger rate. The system is now installed at Shands Hospital at the University of Florida and is undergoing phantom tests in anticipation of future clinical trials.

I. INTRODUCTION

THE University of Florida (UF) and Thomas Jefferson National Accelerator Facility (JLab) are collaborating on the development of a mobile cardiac PET based imager for use in an intensive care/emergency room setting. Often emergency room and intensive care unit patients are in too critical condition to be safely moved to a hospital's nuclear medicine suite to better evaluate their cardiac function. To address this need we have developed and built a mobile cardiac PET based imager for use in an intensive care and emergency room environment. No commercial source exists for a clinical PET

Manuscript received October 26, 2007. The Jefferson Science Associates (JSA) operates the Thomas Jefferson National Accelerator Facility for the United States Department of Energy under contract DE-AC05-06OR23177. Support for this research came from the United States Army Medical Research and Materiel Command under Award No. W81XWH-04-1-0594, the DOE Office of Biological and Environmental Research and from the DOE Office of Nuclear Physics.

A.G. Weisenberger, B. Kross, S. Majewski, J. McKisson, V. Popov, and J. Proffitt are with Jefferson Lab, Newport News, VA, USA, (telephone: 757-269-7090, e-mail: drew@jlab.org).

M.F. Smith is with the University of Maryland, Baltimore, MD, USA, (telephone: 410-328-1320, e-mail: msmith7@umm.edu).

D. Gilland and B. Hammond are with the University of Florida, Gainesville, FL (telephone: 352-846-3066, e-mail: gilland@ufl.edu).

system that can be moved into the limited space in an emergency room or operating room. The company Segami, Inc. does market a portable cardiac SPECT system but requires the patient to be seated [1]. Our goal was not only to develop a high performance system in a compact mobile package, but to also build an economically practical PET imager. Our detector system is patterned after a dual planar PET detector design that others and us have implemented for breast imaging [2, 3 & 4]. We have described earlier the basic design concept of our detector heads for the mobile PET system which are based on position sensitive photomultiplier tubes (PSPMTs) and initial technology testing which we will summarize here. [5, 6 & 7]

The system utilizes a modular design of 16 detector modules based on the compact channel plate-based PSPMT. A total of 16 PSPMTs are used to form a detector head 25 cm x 25 cm in area. The analog signals from the PSPMT are readout and digitized using a JLab developed high rate FPGA based data acquisition ADC system. In Fig. 1 is a photograph of the two detector heads mounted in a mobile gantry at the University of Florida.



Fig. 1. Photograph of 25 cm x 25 cm detector heads attached to mobile gantry installed at the University of Florida.

II. METHODS

Each detector head is composed of sixteen separate PSPMT detector modules. The basic PSPMT detector module is based on a Burle [8] 85002-800 four-pad microchannel plate-based position sensitive photomultiplier tube that provides four high-rate analog outputs. Several PSPMTs in the first batch of Burle 85002-800 failed because of loss of vacuum. The manufacturer was able to modify their manufacturing process to deliver a more robust PSPMT. For each detector head we arrange 16 PSPMT units in which each PSPMT is spaced apart with a 1 cm gap resulting in a 4 x 4 array. Thus each detector head has a 25 cm x 25 cm field of view. Air coupled to the array of PSPMTs is a scintillation array (made by Saint-Gobain Crystals and Detectors [9]) of 5 mm x 5 mm x 12.5 mm NaI(Tl) pixels spaced at 5.5 mm providing a total active area of approximately 25 cm x 25 cm. The pixels are optically separated by white reflective/ diffusive epoxy material. Please see Fig. 2.

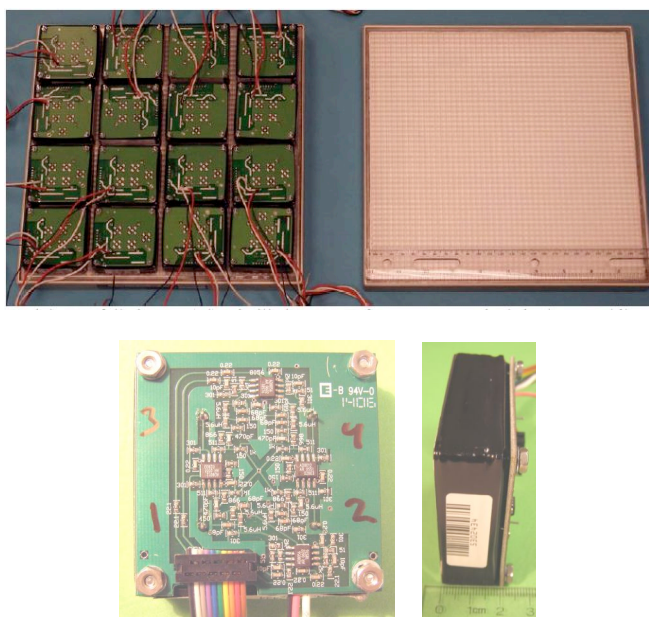


Fig. 2. At top are shown PSPMTs as arranged in a 1 cm spaced configuration to cover the 25 cm x 25 cm FOV of the 5 mm pixel NaI(Tl) scintillation array, pictured separately at top right. In the two bottom pictures a single PSPMT with attached amplifier board is shown in two views. Total thickness of the very compact package PMT+card+connectors is less than 30 mm.

A total of 64 analog outputs are therefore read per detector head thus requiring 128 ADC channels for the whole system. The fast pulse per detector head is formed by summing all 64 pads and producing a corresponding fast constant fraction discriminator trigger pulse for two-head coincidence requirement or single gamma imaging mode trigger. A special interconnect board collects pad signals from individual PSPMTs for transfer via cables to the DAQ system. The board also distributes individually adjusted high voltages (HVs) to

each PSPMT module. The individual HV-PSPMT bias voltages are adjusted to assure that all PSPMT modules in the detector head have similar gain and signal response to the same initial energy deposited (511 keV).

To assure good optical coupling of scintillator pixels opposite the dead regions between the sparsely placed PSPMTs, an additional optical light-guide was added between the 5 mm glass window of the encapsulated NaI(Tl) array and PSPMTs. This light-guide is made of a high quality 20 mm thick UV acrylic plate. Light sharing between the detector modules is achieved by the use of the light-guide resulting in the “dead” regions between PSPMTs resulting in only a 45% drop in signal across the gap. To guarantee long-term optical coupling stability, only dry optical couplings were used between both windows and the PSPMTs. Please see Fig. 3 below for an example of the raw image acquired. We used a ^{22}Na point source to obtain the image.

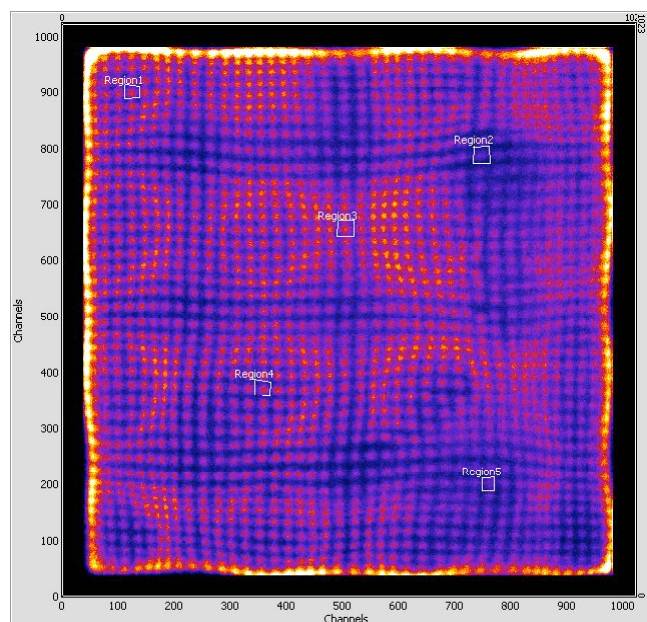


Fig. 3. Example of a raw flood image from a fully illuminated detector head (with a ^{22}Na source) after first-order gain uniformity correction (by adjusting HV biases of individual PMTs). Good pixel separation over the whole field-of-view is observed. Response non-uniformities are still evident because of remaining gain differences, dead regions between individual photomultipliers, and low granularity (~ 2.5 cm) of the PMT pad readout. See Fig.4 for individual energy spectra for the regions of interest for the single crystal elements indicated by white rectangles.

In Fig. 4 is shown the variation of gain and energy resolution across the array. As can be seen all crystal elements show good energy resolution of about 15-20% at the 511 keV photopeak confirming proper operation of the detector across all regions of the active surface. The range of amplitudes of about factor of 2 is observed after first-order adjustment of response uniformity.

To achieve high rate capability, each detector head is connected to a separate JLab developed 64 channel FPGA DAQ card [10]. This card is read out via a USB2 link to a

separate data acquisition PC. Two data acquisition PCs, each used for one detector head, send the collected data files for processing to a next level “event builder” computer.

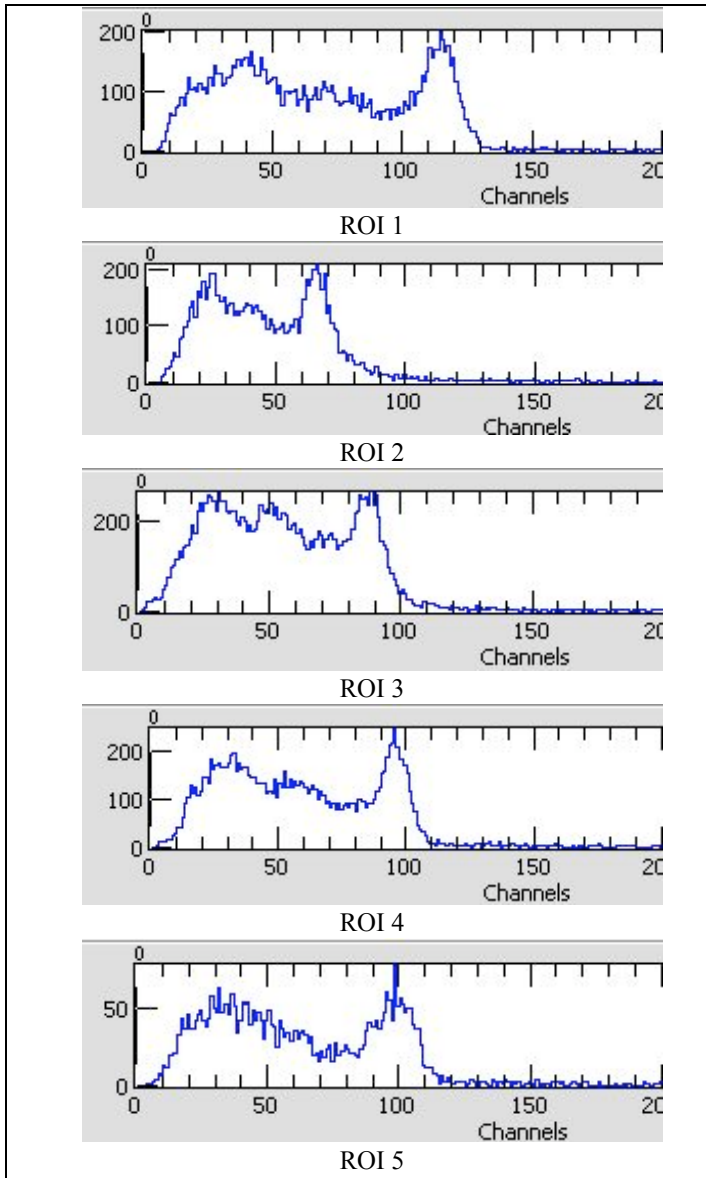


Figure 4: Examples of ^{22}Na energy spectra obtained from selected characteristic five NaI(Tl) crystal elements (corresponding ROIs are shown in the raw image in Fig. 3).

Please see Fig. 5. On the “event builder” computer time-stamped data files are collected separately for each detector head. The pair of files file can be processed and fused into a single coincident file or treated separately when used in a single gamma mode for detector testing.

During the coincident file event building phase, recorded and time-stamped events corresponding to two coincident 511 keV photons from both detector heads are processed and put into a summary file, listing final calculated x and y gamma event positions and gamma ray energies for the two gammas

from both detector heads, plus an event time stamp for each acquired coincident event, with ~ 5 ns time accuracy.

FPGA ADC data acquisition is controlled by distributed Java-based software. Java-based server application sits on each of the acquisition computers and directly controls one FPGA ADC board through a USB2 connection. The USB driver for the FPGA board is directly accessed by C++ code; the JNI (Java Native Interface) is used to allow Java indirect control of the USB driver.

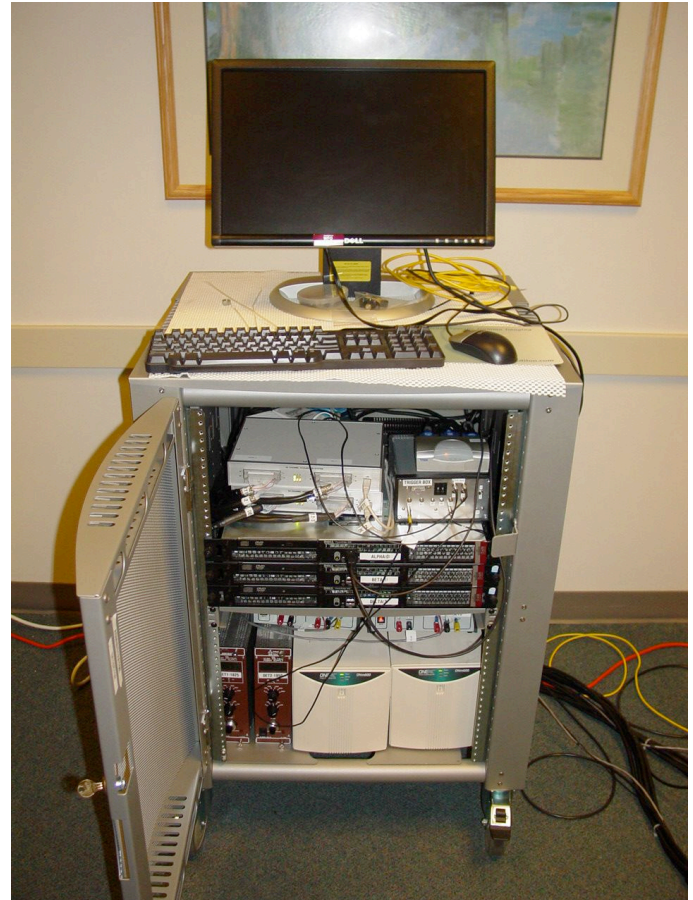


Fig. 5. Photograph of mobile electronics rack. Installed are three rack mounted PCs, two FPGA based ADC modules, low voltage and high voltage power supplies and two hospital grade un-interruptible power supplies with the monitor and keyboard.

The server application on each of these machines is controlled by a remote client Java-based application on the control event builder computer that coordinates the collective acquisition, transfer, and processing of data. The client application is connected to each of the four server applications through a dedicated gigabit Ethernet network. After data is acquired and written to disk on the acquisition computers, the server application transfers data to the remote client computer. Finally, the client application sorts through data from coincident detectors, matches events by the time stamp and then sends the data for reconstruction. Details of the software architecture are described elsewhere at this conference [11].

The software analysis program reads data written to disk by the acquisition software in order to display raw images, implement calibrations and corrections, and provide tools to characterize the two detector head system performances. A special position algorithm uses digitized raw pad signals from all 64 pads of sixteen PSPMTs to obtain raw gamma event positions. Below in Fig 6 is a photograph of the two detectors mounted in the mobile gantry at the University of Florida.

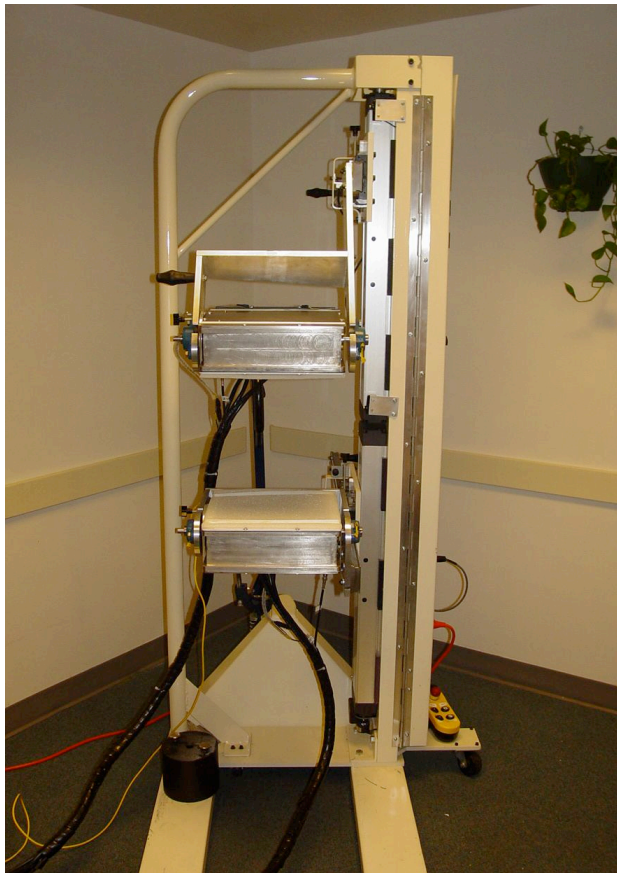


Fig. 6. Photograph of the complete mobile PET imaging system in place at Shands Hospital at the University of Florida.

III. RESULTS

The cardiac imager can operate with over 100 kHz coincidence trigger rate and achieves uniform detection efficiency across the 25 cm x 25 cm FOV, including dead regions between PSPMTs where signal decreases to no less than about 55% relative to the on-PMT signal value. Initial timing resolution of about 5 ns FWHM was achieved for a single detector head (against fast trigger detector). One of the detector heads was shipped back to Jefferson Lab to undergo a PSPMT replacement. The detector head was damaged through shipping. The University of Florida is discussing the incident with United Parcel Service. Once the detector is repaired we intend to continue testing the performance of the system in anticipation of clinical trials.

IV. SUMMARY

We have in place at the University of Florida a mobile cardiac PET based imager for use in an intensive care/emergency room setting. Our system is based on 16 Burle 85000 PSPMTs coupled to a NaI(Tl) scintillating crystal array for each head. The arrays are composed of 5 mm x 5 mm x 12.5 mm thick crystal elements spaced at a 5.5 mm step. Early evaluation tests demonstrated that the imager is a high performance economically practical PET imager system in a compact mobile package. The detectors underwent initial tests at the University of Florida and are report also at this conference [12].

V. ACKNOWLEDGMENT

We thank Bill Gunning for assistance with the electronics fabrication.

VI. REFERENCES

- [1] Segami Corporation, Columbia, MD.
- [2] C. J. Thompson, K. Murthy, R.L. Clancy, J. L. Robar, A. Bergman, R. Lisbona, A. Loutfi, J. H. Gagnon, I. N. Weinberg, R. Mako, "Imaging Performance of PEM-I: A High Resolution System for Positron Emission Mammography (PEM)," Nuclear Science Symposium and Medical Imaging Conference Record, Vol. 2, Pg. 1074-1078, 1995.
- [3] M.F. Smith, S. Majewski, A. G. Weisenberger, D. A. Kieper, R. R. Raylman, T.G. Turkington, "Analysis of factors affecting positron emission mammography (PEM) image formation," IEEE Transactions on Nuclear Science, vol. 50, no. 1, pp: 53-59, Feb. 2003.
- [4] M. F. Smith, S. Majewski, R. R. Raylman, "Positron emission mammography with multiple angle acquisition," Nuclear Science Symposium and Medical Imaging Conference Record, vol. 3, pp: 1883-1886, 2002.
- [5] U.J. Tipnis, D.R. Gilland, M.F. Smith, W.E. Drane, S. Majewski, "Design of a compact, mobile PET detector for bedside cardiac imaging," Nuclear Science Symposium Conference Record, 2003 IEEE, vol 4, pp: 2438 - 2441, 19-25 Oct. 2003.
- [6] S. Majewski, W. Gunning, R. Hammond, B. Kross, M. Smith, V. Popov, J. Proffitt, A. Weisenberger, R. Wojcik, and D. Gilland, "Development and Evaluation of Detector Heads and Readout for a Mobile Cardiac Imager System," presented at 2006 IEEE Nuclear Science Symposium and Medical Imaging Conference.
- [7] U. J. Tipnis, M. F. Smith, T. G. Turkington, J. Wilson, S. Majewski, B. Kross, R. Wojcik, D. R. Gilland, "A simulation study of a bedside cardiac PET imager," Nuclear Science Symposium Conference Record, 2004 IEEE vol. 5, pp 3126-3129, 16-22 Oct. 2004.
- [8] Burle Industries, Lancaster, PA.
- [9] Saint-Gobain Crystals and Detectors, Newbury, OH.
- [10] J. Proffitt, W. Hammond, S. Majewski, V. Popov, R.R. Raylman, A.G. Weisenberger, R. Wojcik, R, "A flexible high-rate USB2 data acquisition system for PET and SPECT imaging," IEEE Nuclear Science Symposium Conference Record, vol. 5, pp: 2971 - 2975, 2005.
- [11] J. E. McKisson, W. Hammond, J. Proffitt, A. G. Weisenberger, "A Java Distributed Acquisition System for PET and SPECT Imaging," presented at 2007 IEEE Nuclear Science Symposium and Medical Imaging Conference.
- [12] M.T. Studenski, J.G. Parker, D. R. Gilland, S. Majewski, W. Hammond, "Performance Evaluation of a Small Field-of-View, Mobile PET/SPECT System," presented at 2007 IEEE Nuclear Science Symposium and Medical Imaging Conference.

Human Subjects Protocol

1. Project Title:

Pre-clinical and Clinical Evaluation of High Resolution, Mobile Gamma Camera and Positron Imaging Devices

2. Investigator(s):

Principal Investigator: David Gilland, Ph.D.
Co-investigator: Walter Drane, M.D.

3. Abstract:

The objective of this study is to evaluate the clinical efficacy of new cardiac imaging device: a compact and mobile positron imaging camera. This device offers an inexpensive alternative to conventional, fixed positron emission tomography (PET) systems, which are typically not readily available to an in-patient population. The proposed device has several advantages over conventional systems including (1) greater flexibility in positioning with respect to the target organ for improved spatial resolution and sensitivity, (2) the ability to image patients who cannot be transported to a radiology suite, (3) the potential for greater cost effectiveness for organ-specific imaging tasks compared with larger, general purpose imaging systems. Our hypothesis is that the proposed PET system can provide images of cardiac function that can enable the diagnosis of hibernating myocardium at a level comparable to the more expensive systems. In addition, the proposed system will have the mobility and compact size that will enable the system to more readily image an in-patient population, for example, patients under intensive care.

The images obtained from patients with the proposed imaging system will be validated against conventional PET images and/or magnetic resonance (MR) images, which are currently considered the gold standard imaging techniques for assessing cardiac function. This study will select approximately twenty patients with established diagnosis of coronary artery disease who have had, or will have, conventional PET and/or MR cardiac imaging procedures as a part of their normal clinical work-up. These patients will be imaged with the proposed device, and the results of these procedures will be compared. In addition, for patients that ultimately undergo surgical revascularization, the subsequent outcome of their cardiac function will serve as a gold standard for evaluating the accuracy of the imaging results.

4. Background:

For improved management of patients with known coronary artery disease, it is critical to distinguish scarred from “hibernating” myocardium. Hibernating

myocardium refers to an area of the heart muscle that has chronically reduced blood flow at rest but is metabolically alive. With this condition, improved cardiac function typically occurs after surgical revascularization (e.g. stent placement or by-pass procedure) and long-term survival is greatly increased; whereas with the scarred condition, surgical intervention is not effective at improving function. Without knowledge of hibernating myocardium the only treatment is medical support or cardiac transplant.

Several imaging options are available to detect hibernating myocardium. Standard rest-stress perfusion imaging is a relatively low-cost alternative. The problem with this approach is that approximately 25-50% of cases that demonstrate fixed defects (defects in both rest and stress studies) are incorrectly called scar tissue when in reality it is hibernating myocardium. A more accurate, but more expensive, imaging option is cardiac PET or MR. The current gold standard is PET; however, because of the greater expense of PET, many institutions are using MR to detect hibernating myocardium. Delayed enhancement on gadolinium MR is a sign of irreversible damage; otherwise, hibernating myocardium is suggested.

The imaging device that is being tested in this study is designed to be a lower cost alternative to conventional, fixed PET systems but one that can deliver images that can enable the diagnosis of hibernating myocardium at a level comparable to the more expensive systems. The cost has been reduced by using less expensive technologies but ones that can deliver satisfactory performance for the task at hand. In addition, the proposed system will have the mobility and compact size that will enable the system to more readily image an in-patient population, for example, patients under intensive care.

Currently, there is not a commercial imaging system available that has the capabilities that have been designed into the proposed system. There are compact and mobile imaging systems that are designed for standard rest-stress gamma imaging, but not PET. Also, these systems do not have the capability to image critically ill patients.

5. Specific Aims:

The specific aim of this study is to evaluate the capability of a novel PET imaging system to diagnosis hibernating myocardium in patients with known coronary artery disease. The overall objective of the study is to quantify the level of agreement in the results obtained from the new imaging system with those obtained from a conventional PET or MR imaging system.

6. Research Plan:

6.1 Study Design

Images will be obtained from the subjects of this study using the experimental device, and the results will be interpreted by a nuclear medicine physician. Either prior or subsequent to this procedure, the subject will undergo a cardiac PET or MR procedure as part of their standard of care treatment. Interpretation of the PET or MR images will be independent of the experimental results. The two results will be quantitatively compared in terms of the presence, location and extent of hibernating myocardium. Approximately 20 subjects will be recruited in order to obtain a reasonable certainty in the measured correlation.

6.2 Study Location

The study will be performed at the Veterans Affairs Medical Center (VAMC) adjacent to the University of Florida Shands Hospital. This medical center has the larger volume of severely diseased patients with potential hibernating myocardium compared to UF Shands Hospital. A new, state-of-the-art PET system is anticipated to be installed within the next nine months. The imaging will be performed either within the nuclear medicine clinic or in the ward that the patient is being treated.

6.3 Subject Recruitment Procedure

Appropriate patients for this study will be identified by a VAMC staff cardiologist (Dr. Carsten Schmalfluss) with consultation from Dr. Walter Drane. The patients typically will present with an ejection fraction of less than 35% and have a known history of coronary artery disease with suspected hibernating myocardium. Typically, patients will have already undergone tests to evaluate myocardial perfusion state. Dr. Schmalfluss will advise the patient on the details of the study, including benefits and risks, before obtaining consent.

6.4 Inclusion/Exclusion criteria:

INCLUSION CRITERIA

1. The subjects (or legally authorized representative) understand the nature of the study and provide written informed consent prior to data collection.
2. Male subjects or non-pregnant women (females of child bearing potential must have a negative pregnancy test prior to enrollment to the study).
3. Subjects age from 40 to 80 years old.

4. Subjects with:
 - a. diagnosis of coronary artery disease
 - b. ejection fraction less than 35%
 - c. suspected hibernating myocardium
5. Subjects with serum creatinine ≤ 1.5 md/dl.
6. Subjects who are willing to comply with the protocol requirements and specified follow-up evaluations.

EXCLUSION CRITERIA

1. Pregnant women
2. Subjects with serum creatinine ≥ 1.5 md/dl
3. Subjects who have known allergy or sensitivity to iodine contrast media
4. Patients with life expectancy less than several months.

6.5 Imaging Procedure

Patients will be prepped for the study in the standard manner for cardiac PET imaging. The patient is fed a high glucose meal, then shortly after injected with a dose of F-18-FDG (the standard cardiac PET imaging agent). Typically, this dose is 7-15 milliCuries; however, the exact dose for these studies will be determined by phantom experiments yet to be performed. After 90 minutes, the imaging is performed, which will typically last 20-30 minutes. This will be a one-time procedure for each patient in the study.

6.6 Protection of Subject Medical Information

A list with the subjects' identifiers (name, medical record number) will be created. The subjects will be assigned an alpha-numeric code which will be linked to the identifier list. This list will be kept in a locked compartment in the Principal Investigator's office, being accessible only to the Principal and Co-Principal Investigators.

7. Possible Discomforts and Risks:

The discomforts and risks for subjects participating in this study are equivalent to those experienced during routine PET procedures. Those include possible bruising at the injection site and a standard radiation dose involved in PET procedures. Subjects will not be charged financially for participating in this study.

8. Possible Benefits

The possible benefit to the patient for participating in this study is minimal but includes the additional information on the state of their coronary artery disease that arises from an independent diagnostic exam.

9. Conflict of Interest

There is no potential benefit to the Principal Investigator or Co-principal Investigator beyond the professional benefit from academic publication and presentation of this study's results.